

RESEARCH ARTICLE SUMMARY

CELL BIOLOGY

Phase separation of a yeast prion protein promotes cellular fitness

Titus M. Franzmann, Marcus Jahnel, Andrei Pozniakovsky, Julia Mahamid, Alex S. Holehouse, Elisabeth Nüske, Doris Richter, Wolfgang Baumeister, Stephan W. Grill, Rohit V. Pappu, Anthony A. Hyman,* Simon Alberti*

INTRODUCTION: The formation of dynamic, membraneless compartments using intracellular phase transitions such as phase separation and gelation provides an efficient way for cells to respond to environmental changes. Recent work has identified a special class of intrinsically disordered domains enriched for polar amino acids such as glycine, glutamine, serine, or tyrosine as potential drivers of phase separation in cells. However, more traditional work has highlighted the ability of these domains to drive the formation of fibrillar aggregates. Such domains are also known as prion domains. They have first been identified in budding yeast proteins that form amyloid-like aggregates. Because these aggregates are heritable and change the activity of the prion-domain-containing protein, they are thought to be a common mechanism for phenotypic inheritance in fungi and other organisms. How-

ever, the aggregation of prion domains has also been associated with neurodegenerative diseases in mammals. Therefore, the relationship between the role of these domains as drivers of phase separation and their ability to form prion-like aggregates is unknown.

RATIONALE: The budding yeast translation termination factor Sup35 is an archetypal prion-domain-containing protein. Sup35 forms irreversible heritable aggregates, and these aggregates have been proposed to be either a disease or an adaptation that generates heritable phenotypic variation in populations of budding yeast. Despite having been described almost 25 years ago, the physiological functions of the Sup35 prion domain and other prion-like domains remain unclear. Uncovering these functions is a prerequisite for understanding the evolutionary pressures shaping prion-like se-

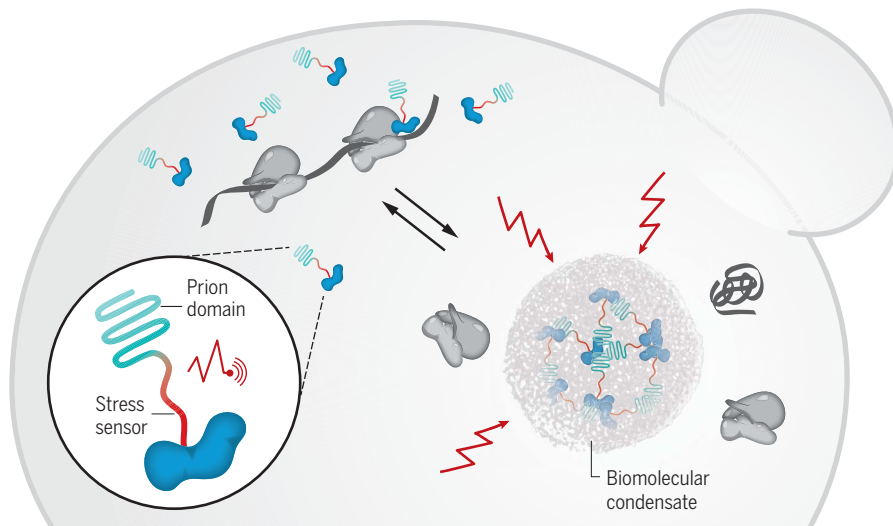
quences and how their physiological and pathological transitions affect cellular fitness.

RESULTS: Here, we show that the prion domain of Sup35 drives the reversible phase separation of the translation termination factor into biomolecular condensates. These condensates are distinct and different from fibrillar amyloid-like prion particles. Combining genetic analysis in cells with in vitro reconstitution protein biochemistry and quantitative biophysical methods, we demonstrate that Sup35 condensates form by pH-induced liquid-like phase separation as a response to sudden stress.

The condensates are liquid-like initially but subsequently solidify to form protective protein gels. Cryo-electron tomography demonstrates that these gel-like condensates consist of cross-linked Sup35 molecules forming a porous meshwork. A cluster of negatively charged amino acids functions as a pH sensor and regulates condensate formation. The ability to form biomolecular condensates is shared among distantly related budding yeast and fission yeast. This suggests that condensate formation is a conserved and ancestral function of the prion domain of Sup35. In agreement with an important physiological function of the prion domain, the catalytic guanosine triphosphatase (GTPase) domain of the translation termination factor Sup35 readily forms irreversible aggregates in the absence of the prion domain. Consequently, cells lacking the prion domain exhibit impaired translational activity and a growth defect when recovering from stress. These data demonstrate that the prion domain rescues the essential GTPase domain of Sup35 from irreversible aggregation, thus ensuring that the translation termination factor remains functional during harsh environmental conditions.

CONCLUSION: The prion domain of Sup35 is a highly regulated molecular device that has the ability to sense and respond to physicochemical changes within cells. The N-terminal prion domain provides the interactions that drive liquid phase separation. Phase separation is regulated by the adjacent stress sensor. The synergy of these two modules enables the essential translation termination factor to rapidly form protective condensates during stress. This suggests that prion domains are protein-specific stress sensors and modifiers of protein phase transitions that allow cells to respond to specific environmental conditions. ■

The list of author affiliations is available in the full article online.
*Corresponding author. Email: alberti@mpi-cbg.de (S.A.); hyman@mpi-cbg.de (A.A.H.)
Cite this article as T. M. Franzmann et al., *Science* 359, eaao5654 (2018). DOI: 10.1126/science.aao5654



The Sup35 prion domain regulates phase separation of the translation termination factor Sup35 during cellular stress. The translation termination factor Sup35 (depicted in the magnifying glass) consists of a disordered prion domain (cyan) a disordered stress sensor domain (red) and a folded catalytic domain (blue). During growth, Sup35 catalyzes translation termination. During cell stress, the prion domain and the sensor domain act together to promote phase separation into protective and reversible biomolecular condensates.

RESEARCH ARTICLE

CELL BIOLOGY

Phase separation of a yeast prion protein promotes cellular fitness

Titus M. Franzmann,¹ Marcus Jahnel,^{1,2} Andrei Pozniakovsky,¹ Julia Mahamid,³ Alex S. Holehouse,⁴ Elisabeth Nüske,¹ Doris Richter,¹ Wolfgang Baumeister,⁵ Stephan W. Grill,^{1,2} Rohit V. Pappu,⁴ Anthony A. Hyman,^{1*} Simon Alberti^{1*}

Despite the important role of prion domains in neurodegenerative disease, their physiological function has remained enigmatic. Previous work with yeast prions has defined prion domains as sequences that form self-propagating aggregates. Here, we uncovered an unexpected function of the canonical yeast prion protein Sup35. In stressed conditions, Sup35 formed protective gels via pH-regulated liquid-like phase separation followed by gelation. Phase separation was mediated by the N-terminal prion domain and regulated by the adjacent pH sensor domain. Phase separation promoted yeast cell survival by rescuing the essential Sup35 translation factor from stress-induced damage. Thus, prion-like domains represent conserved environmental stress sensors that facilitate rapid adaptation in unstable environments by modifying protein phase behavior.

The formation of dynamic, membraneless compartments via intracellular phase transition provides an efficient way for cells to respond to metabolic changes (1, 2). This is because phase transitions are sensitive to small changes in physicochemical conditions, such as the cytosolic pH, which are a readout of metabolic state. Recent work has identified prion-like sequences as drivers of phase separation of protein compartments in cells (3–6). However, more traditional work has highlighted the ability of prion-like domains to form fibrillar assemblies that are thought to drive heritable phenotypic variation (7–9). Studies in humans and other mammals have implicated fibrillar assemblies of prion-like proteins in age-related neurodegeneration (10). Despite having been described almost 25 years ago (11), the physiological functions of prion-like sequences remain unclear. Uncovering this physiological function is an essential and important prerequisite for understanding whether the fibrillar assemblies are purely pathological or whether they have functional relevance.

Cells respond to stress by arresting the cell cycle, shutting down metabolism, and inducing stress-protective pathways. Upon cessation of stress, they must rapidly reprogram their me-

tabolism and restart growth and division. When cells are stressed, they stop translation and release translation factors and mRNAs from polyosomes that are subsequently sequestered in granules (12, 13). After removal of stress, mRNAs reassociate with ribosomes, and translation factors ensure proper restart of protein synthesis.

The prion protein Sup35 forms reversible biomolecular condensates in stressed yeast cells

One of the key factors of protein synthesis is the protein Sup35, a translation termination factor. Sup35 is an archetypal prion domain-containing protein. Numerous studies over the past 25 years have shown that the prion domain of Sup35 forms heritable, mainly fibrillar aggregates. Consistent with this idea, when we depleted yeast of energy (see the supplementary materials), Sup35 assembled into submicrometer-scaled particles (Fig. 1A). Particle formation coincided with arrested cell growth, and cells persisted in the arrested state for as long as particles were present (Fig. 1B and movie S1).

However, a number of observations suggested that Sup35 did not actually form amyloid-like prion aggregates. First, Sup35 particles dissolved within a few minutes of removing energy stress when cells started growing (Fig. 1, A and B, and movie S1). Sup35 particles also formed in stationary phase yeast and dissolved after cells were supplied with fresh medium (Fig. 1C and fig. S1A). Neither formation nor dissolution of Sup35 particles depended on the molecular chaperone Hsp104, which is required for propagation of Sup35 prion particles (14) (fig. S1B). Furthermore, the stress-induced Sup35 particles did not have any of the biochemical features of amyloid-like aggregates (fig. S1, C and D). This suggests that stress-inducible Sup35 assemblies

were not bona fide prion particles but may instead be biomolecular condensates (1, 15) that formed reversibly upon stress.

Starved and energy-depleted yeast experience a reduction in cytosolic pH (16). Likewise, the cytosolic pH of stationary phase cells was acidic (fig. S1, E and F). By manipulating the cytosolic pH with the proton carrier 2,4-dinitrophenol (DNP) (16–18), we found that acidification was sufficient to induce Sup35 condensates (Fig. 1E). The condensates did not colocalize with the stress granule protein Pab1 in stationary phase cells, and partial colocalization was found in pH stressed cells (fig. S1A and G). Thus, physiological pH changes regulate the formation of reversible Sup35 condensates.

Sup35 condensates form by pH-dependent phase separation and gelation

To provide a mechanistic understanding of pH-regulated condensation, we purified Sup35 and reconstituted the condensates in vitro. When 2 μ M of purified Sup35 was incubated in physiological buffer, the protein remained diffuse (Fig. 2, A and B, and fig. S2A). However, when the pH was reduced from 7.5 to 6.0, condensates of Sup35 formed (Fig. 2, A and B, and fig. S2, B to D). Sup35 condensates adopted spherical shapes in solution and deformed when contacting the microscope slide (fig. S2B), suggesting that they are liquid-like. Supporting this idea, two Sup35 drops fused when brought together with an optical tweezer (Fig. 2C and movie S2), and photobleached regions within a Sup35 condensate quickly recovered fluorescence (Fig. 2D).

Using fluorescence recovery after photobleaching, we found that Sup35 was mobile in growing cells; it became immobile when sequestered into condensates, upon stress (Fig. 1D). We confirmed this behavior in vitro, where Sup35 initially phase-separated to form liquid droplets but then solidified into a gel-like state as suggested by fusion and photobleaching experiments (Fig. 2D and fig. S2, E to G). Cryo-electron tomography of Sup35 droplets revealed that gel-like droplets consisted of an amorphous, yet well-defined, meshwork with an average mesh size of \sim 10 nm (Fig. 2E; fig. S2, H to K; and movie S3). Such meshwork has not been seen in droplets formed by well-described stress and P granule proteins (3, 19). Gel-like condensates dissolved when the salt concentration or pH was raised or in the presence of small amounts of detergents, demonstrating reversibility in vitro (fig. S3, A to E). Thus, changes in pH regulate the formation of Sup35 into liquid droplets, which subsequently solidify.

The disordered M domain is a stress sensor that regulates phase separation of Sup35

The N-terminal region of Sup35 is intrinsically disordered and can be divided into two parts: an N-terminal prion domain (N) and a charged middle domain (M) (20, 21) (Fig. 2F). The conserved C-terminal guanosine triphosphatase (GTPase)

¹Max Planck Institute of Molecular Cell Biology and Genetics, Pflotenauerstrasse 108, 01307 Dresden, Germany. ²Biotec, Technische Universität Dresden, Tatzberg 47/48, 01307 Dresden, Germany. ³European Molecular Biology Laboratory, Heidelberg, Meyerhofstrasse 1, 69117 Heidelberg, Germany. ⁴Department of Biomedical Engineering and Center for Biological Systems Engineering, Washington University in St. Louis, St. Louis, Missouri, USA. ⁵Max Planck Institute of Biochemistry, Department of Molecular Structural Biology, Am Klopferspitz 18, 82152 Martinsried, Germany. *Corresponding author. Email: alberti@mpi-cbg.de (S.A.); hyman@mpi-cbg.de (A.A.H.)

domain (C) is essential and catalyzes termination of protein synthesis. The N and M domains are dispensable, but conservation of the NM domain (22–25) indicates that they form a bipartite functional unit with an important function, which to date remains undefined.

A minimal module consisting only of the prion (N) and the M domain (NM) formed droplets in a reversible and pH-dependent manner in vitro (Fig. 2I, fig. S3F, and movie S4). The sequence of the M domain has a linear cluster of ionizable groups, specifically glutamic acid residues, located at the C-terminal end (Figs. 2F and 3A). Removing the charges within the negative cluster (Sup35M3 variant) yields a fully functional Sup35 variant (fig. S3, G and H) but with altered phase behavior, such that protein-rich droplets formed at pH 7.5 and the pH dependence of droplet formation was discernibly reduced in vitro (Fig. 2G) and in vivo (Fig. 2H and fig. S3I). Thus, pH sensing of Sup35 is facilitated by its charged M domain through protonation of glutamates. We propose that the high density of acidic residues in the M domain causes an upshift in the pK_a value of glutamic acid (where K_a is the acid dissociation constant),

which is normally ~ 4.1 (26). This is consistent with recent studies demonstrating up-shifted pK_a values in acidic tracts of disordered proteins (27)

We next dissected the role of the individual Sup35 domains. The isolated C domain formed interconnected irreversible aggregates at all tested pH conditions (28) (Fig. 2I and fig. S3, J to L). In the presence of the M domain, the extent of irreversible aggregation was strongly reduced, in agreement with a solubilizing role of M (fig. S3L). The presence of M also partially restored condensate formation, but the amount of condensate formed was an order of magnitude lower than for the wild-type protein (Fig. 2I and fig. S3, L and M). Thus, the NM domain helps maintain the solubility of, and provides the pH sensitivity for, the C-terminal termination factor, in which the N domain provides the cohesiveness required for condensation. In other words, the disordered NM domain alters the phase behavior of the C domain by promoting the formation of reversible gels instead of irreversible aggregates. This phenomenon is consistent with the ideas of Semenov and Rubinstein, who predicted that gelation is driven by phase separa-

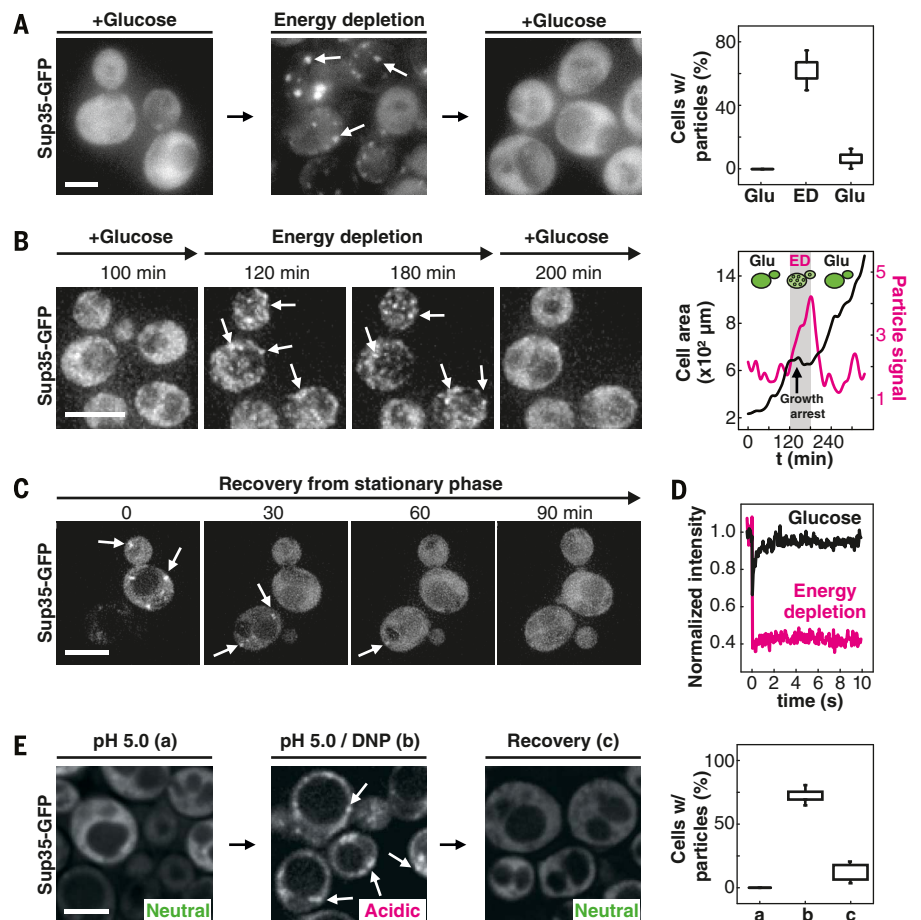
tion for so-called associative polymers (29). This phenomenon has been predicted to be relevant for linear multivalent proteins (30), and it appears to apply to Sup35 as well.

Phase separation of Sup35 but not prion formation is conserved among distantly related yeast

The charge distribution, but not the sequence within the Sup35 M domain, is conserved across diverse fungi (Fig. 3A, fig. S4A, and table S1). Indeed, Sup35 from *Schizosaccharomyces pombe* exhibited similar behavior compared with that of *Saccharomyces cerevisiae*; in vivo, it formed stress-dependent intracellular condensates (Fig. 3, B and C, and fig. S4B), and in vitro, it formed reversible liquid droplets at low pH (Fig. 3, D to G; fig. S4, C to G; and movie S5) that cross-link into a meshwork that was indistinguishable from the one of Sup35 from *S. cerevisiae* (Fig. 3H; figs. S4, H to J; and movie S6). Importantly, and in contrast to *S. cerevisiae*, *Sc. pombe* is unable to induce and propagate the prion state of Sup35 (25). Thus, condensate formation, but not prion formation, is conserved among distantly related yeast that diverged more than

Fig. 1. Sup35 forms reversible condensates in *S. cerevisiae*.

(A) Fluorescence images of *S. cerevisiae* expressing green fluorescent protein (GFP)-labeled Sup35 during exponential growth (left), during energy depletion (middle), and after recovery from energy depletion (right). Energy depletion causes reversible condensation of Sup35 into intracellular puncta. White arrows point toward Sup35 condensates. The graph on the right shows a quantification of the cells with particles. About 150 to 200 cells per condition were used for quantification. (B) Fluorescence images taken from a time-lapse movie (see movie S1) of *S. cerevisiae* growing in a microfluidic device (CellAsic). Cells were grown in synthetic complete media for 2 hours. After 120 min, cells were energy-depleted to form Sup35 condensates. Condensates persisted during energy depletion and dissolved when the cells were recovered by being supplied with fresh synthetic medium. White arrows point toward Sup35 condensates. Cell growth was measured as the total increase in occupied area (cell area) as a function of time (t) (black). For particle signal, the maximum fluorescence signal was divided by the minimum fluorescence signal (magenta). Energy depletion coincides with growth arrest and Sup35 condensation. (C) Fluorescence images of *S. cerevisiae* expressing GFP-labeled Sup35 during recovery from stationary phase. Cells were grown to stationary phase for 2 days. White arrows point toward Sup35 particles. Supplying cells with growth medium (t_0) caused dissolution of intracellular condensates and restart of cell growth. (D) The intracellular mobility of Sup35 was accessed by fluorescence recovery after photobleaching. The recovery of fluorescence of GFP-labeled Sup35 was measured in exponentially growing (black) and energy-depleted (magenta) cells. (E) Fluorescence images of *S. cerevisiae* expressing GFP-labeled Sup35 in 100 mM phosphate, pH 5 (left), 100 mM phosphate buffer, 2 mM DNP, pH 5 (middle), and after 60 min of recovery with synthetic complete medium (right). About 150 to 200 cells were used for quantification of each condition. Box indicates intracellular pH as described by Munder *et al.* (16). Scale bar, 5 μm .



400 million years ago and suggests that condensate formation may be the ancestral function of the prion domain of Sup35.

Taken together, our data show that Sup35 forms condensates by pH-dependent phase separation and subsequent gelation into a porous polymer meshwork. The intrinsic disorder of the prion domain likely provides the necessary flexibility for the formation of the meshwork, whereas the precise interactions that cross-link the gel remain to be elucidated (31).

Phase separation rescues the catalytic domain of Sup35 from stress-induced damage

To look at the role of the NM domain during the stress response in yeast, we compared the fitness of cells expressing similar levels of full-length Sup35 and the C domain alone (Sup35C) (fig. S5A). We also monitored the aggregation state of the proteins. Cells expressing only the C domain grew without a noticeable growth defect

in the absence of stress (Fig. 4, A and B), and at the same time the protein was diffuse and soluble (Fig. 4C). Thus, the C domain is not aggregation-prone in the cellular environment, presumably because of the presence of ligands such as guanosine 5'-triphosphate (GTP) (28) (fig. S2A). After stress, the C domain aggregated in a manner that was similar to that of the full-length protein (Fig. 4D). However, after removal of stress, Sup35 condensates dissolved within minutes in wild-type cells. In contrast, in Sup35C cells, dissolution of aggregates could take several hours (Fig. 4, C and D, and fig. S5B). This suggests that the NM domain determines the material properties (reversible gel versus irreversible aggregate) of Sup35 in vivo. Concomitantly, Sup35C cells took longer to restart growth (Fig. 4, A and C, and movies S7 and S8) and exhibited reduced fitness when recovering from stationary phase (Fig. 4B).

Sup35 catalyzes an essential step during protein synthesis, namely translation termination. Indeed, translation was shut down upon energy

depletion, as indicated by polysome disassembly (fig. S5, C and D). This coincided with Sup35 condensation. Conversely, dissolution of Sup35 condensates coincided with polysome reformation (fig. S5, C and D). Importantly, translation activity was specifically impaired after energy depletion in recovering Sup35C cells but not in control cells (Fig. 4E).

The prion state interferes with Sup35 condensate formation and impairs recovery of yeast from stress

How does the prion state of Sup35 affect the ability of cells to recover from stress? To investigate this, we compared prion-containing [*PSI+*] with prion-free [*psi-*] cells for their ability to regrow from the stationary phase (32). [*PSI+*] cells grew without a noticeable defect under normal conditions, but they showed a growth delay after recovery from stationary phase that was similar to that of Sup35C cells (Fig. 4F and fig. S5E). This suggests that the formation

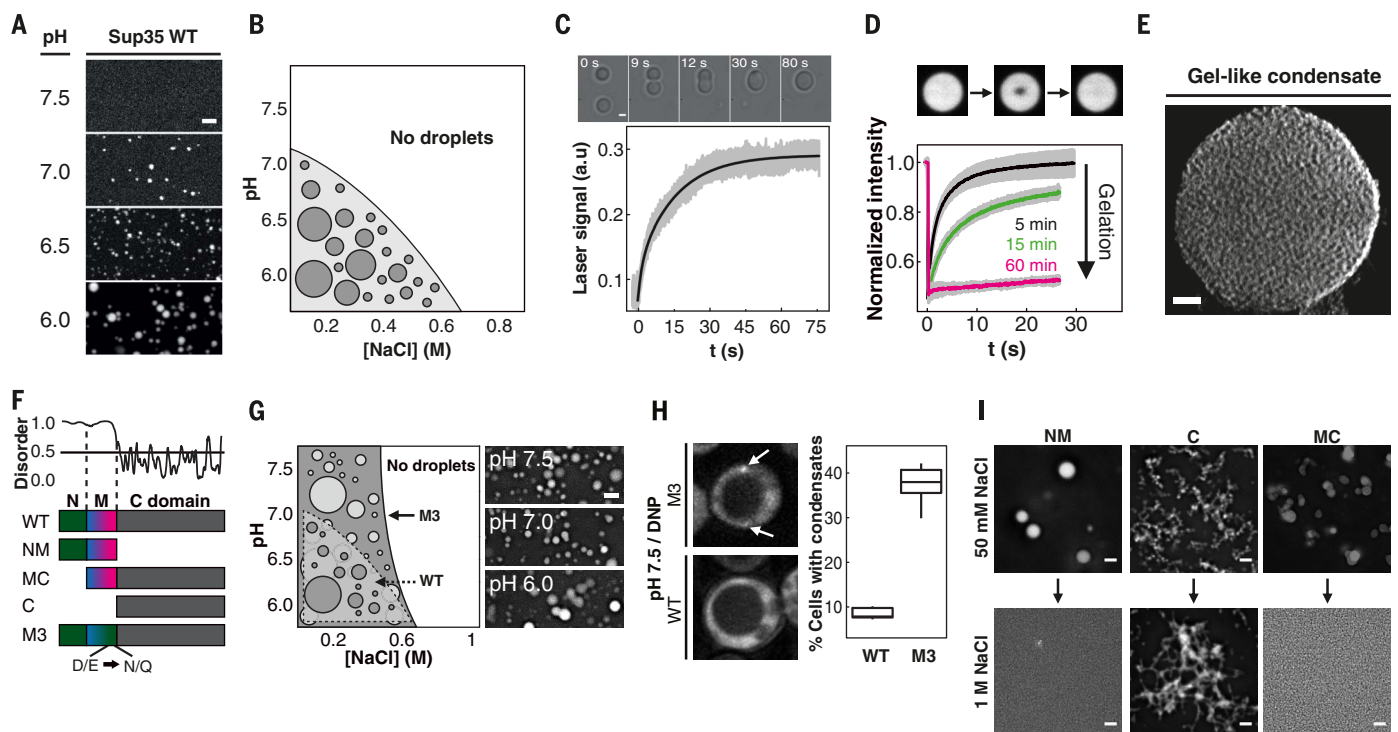


Fig. 2. The Sup35 prion domain synergizes with a pH sensor to drive phase separation into biomolecular condensates. (A) Fluorescence images of 2 μ M GFP-labeled wild-type (WT) Sup35 at indicated pH. Scale bar, 2 μ m. (B) Phase diagram of 2 μ M WT Sup35 with pH and salt concentration as order parameters. Phase separation was scored by the presence or absence of droplets in the samples. (C) Fusion of two Sup35 droplets at pH 6.0. Still images are shown on top. A force curve is shown at the bottom. Scale bar, 2 μ m. (D) Internal rearrangement of Sup35 molecules was assayed by fluorescence recovery after photobleaching as a function of gelation time. A single pixel spot was bleached, and the change in the fluorescence was analyzed as a function of time. Still images are shown before and after bleaching. The drop size was \sim 3 μ m. Analysis of the fluorescence recovery of 5-min-old (black; $N = 19$), 15-min-old (green; $N = 9$), and 60-min-old (magenta; $N = 11$) drops are shown. SD depicted as gray shadow. (E) Three-dimensional (3D)-rendered volume of WT Sup35

gel-like droplet imaged with cryo-electron tomography. Scale bar, 50 nm.

(F) Disorder analysis (top) and schematic of the *S. cerevisiae* Sup35 domain structure. N (N) and middle (M) domain are disordered. The C-terminal domain is folded. Color gradient in M depicts the net charge along the sequence (blue, positive; magenta, negative; green, neutral). (G) Phase diagram of 2 μ M Sup35M3 variant with pH and salt concentration as order parameters. Dashed line indicates the phase diagram of Sup35 WT as shown in (B). Representative images of 2 μ M Sup35M3-GFP at indicated pH shown. Scale bar, 2 μ m. (H) Fluorescence images and quantification of *S. cerevisiae* expressing Sup35M3 (top) and Sup35 WT (bottom) in 40 mM PIPES, pH 7.5, 2 mM DNP. Sup35M3 forms condensates at neutral pH, whereas WT stays diffuse. (I) Phase separation of Sup35 variants was probed at 2 μ M final protein concentration (top). Dissolution was tested by increasing the salt concentration from 50 to 1000 mM NaCl (bottom). Scale bar, 2 μ m.

of stress-protective Sup35 condensates is impaired in the presence of the prion and that [PSI⁺] cells have a reduced fitness when recovering from stress. This demonstrates that the ribosome critically depends on the availability of Sup35 after stress. Taken together, these experiments show that the NM domain provides the catalytic C domain of Sup35 with the ability to recover rapidly from stress, and thus ensures a critical step in restarting translation (Fig. 5).

Discussion

Sup35 is a prominent member of a class of proteins with prion-like domains. These are low-complexity protein domains that consist primarily of polar and aromatic amino acids. They are called prion-like domains because they have been associated with the ability of proteins to spread through yeast populations in a prion-like manner (33). Indeed, numerous studies have highlighted the aggregation potential of prion-like domains when

studied in isolation. Our data suggest that the prion domain, in the context of the full-length protein, adopts a benign role by increasing the solubility of the C-terminal catalytic domain at neutral pH and promoting Sup35 phase separation and gelation under stress. Thus, reversible gel formation, but not prion formation, is likely the ancestral function of the prion domain of Sup35. In agreement, many de novo formed variants of Sup35 prions cause cellular toxicity, suggesting that the prion state could be a sporadically occurring disease (34–37). Prion states may thus be a frequently occurring epiphenomenon of condensate-forming domains, which may or may not have adaptive value.

More generally, organisms must adapt to sudden changes in the environment, independent of transcriptional and translational regulation. In agreement with previous conjectures (38), we suggest that prion domains are protein-specific stress sensors and modifiers of phase transitions

that allow cells to respond to specific environmental conditions. In the case of Sup35, this condition is the lowering of the cytosolic pH under energy stress. However, yeast contains more than 200 proteins with predicted prion-like domains, and *Dictyostelium* contains more than 1000 such proteins (39, 40). It seems likely that organisms deploy prion-like domains to generate protein-specific environmental responses. In agreement, another prion-like domain has recently been shown to tune the phase behavior of the yeast stress granule protein Pab1 (5). Prion domains are therefore crucial stress-adaptive regions that allow organisms to explore and persist in stressful and unstable environments.

Materials and methods

Strains and culture conditions

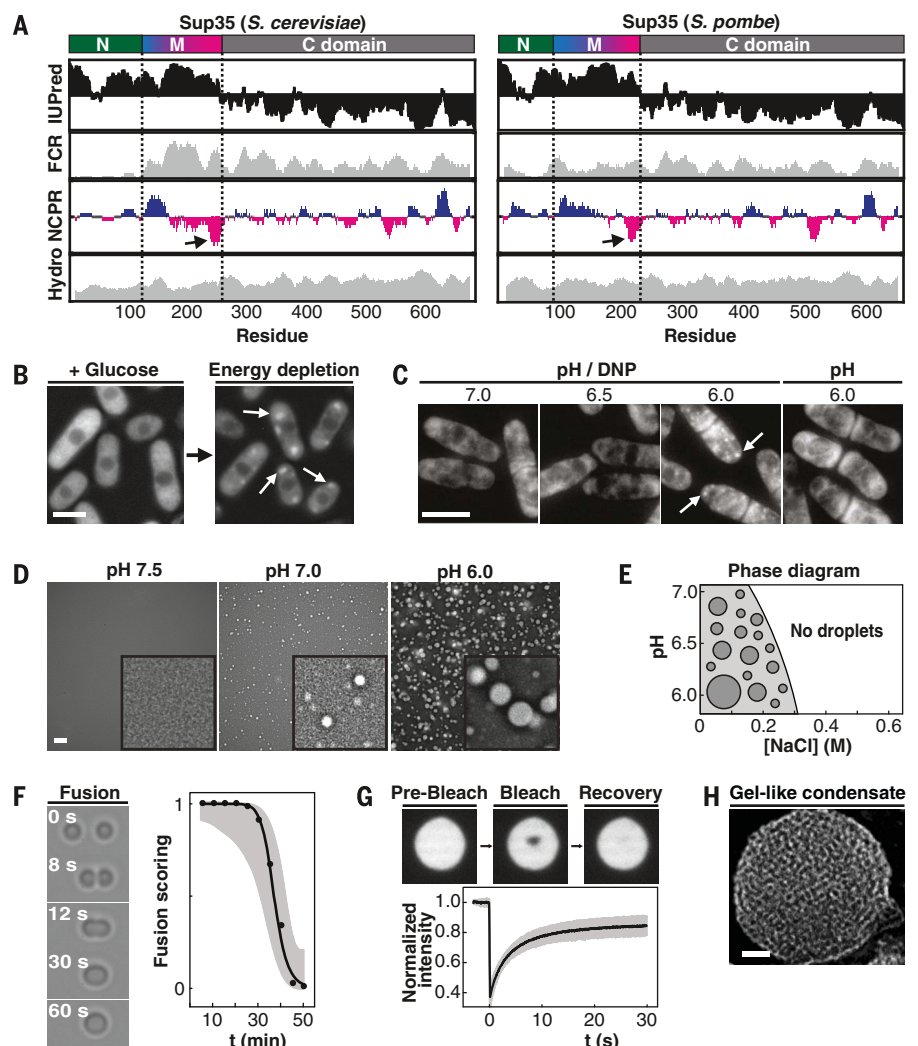
S. cerevisiae was grown at 30°C in yeast extract peptone dextrose (YPD), synthetic complete (SC) or synthetic dropout (SD) medium. *Sc. pombe*

Fig. 3. Phase separation of Sup35 is conserved in the evolutionarily distant fission yeast *Sc. pombe*.

(A) Comparative bioinformatic analysis of Sup35 from *S. cerevisiae* (left) and *Sc. pombe* (right). Sup35 has three domains. The N (green) and M (blue-magenta) domains are predicted to be disordered, and the C domain (gray) is a folded and conserved GTPase domain (degree of predicted disorder; IUPred). FCR, fraction of charged residues; NCP, net charge per residue; Hydro, hydrophobicity. M is disordered and contains a high density of charged residues with a blocky architecture. It carries an overall net negative charge with a net positive charge at the N-terminal half and a strong net negative charge at the end of M. Arrows point toward the M3 charge cluster. (B) Fluorescence images of *Sc. pombe* expressing mCherry-labeled Sup35 grown in medium (left) and after 30 min of energy depletion (right). Scale bar, 5 μ m. (C) Fluorescence images of *Sc. pombe* expressing mCherry-labeled Sup35 exposed to 100 mM phosphate buffer in the presence or absence of DNP at indicated pH. Scale bar, 5 μ m. (D) Fluorescence images of 2 μ M *Sc. pombe* Sup35 in 20 mM PIPES; 3% polyethylene glycol (PEG), 50 mM NaCl at indicated pH. Scale bar, 2 μ m. (E) Phase diagram of Sup35 WT from *Sc. pombe* with pH and salt concentration as order parameters. Phase separation of 2 μ M Sup35 was scored by the presence or absence of droplets in the respective sample.

(F) Controlled fusion experiment of two *Sc. pombe* Sup35 droplets using a dual-trap optical tweezer. Still images show fusion of two Sup35 WT droplets (left). Upon contact, Sup35 droplets fuse and coalesce into one spherical droplet. Size of droplets \sim 3 μ m. Solidification of *Sc. pombe* Sup35 WT was assayed by their ability to fuse with each other as a function of time. Successful fusion was scored 1, when droplets coalesced into a new spherical droplet within 30 s (right).

(G) Internal rearrangement of *Sc. pombe* Sup35 WT molecules was assayed by fluorescence recovery after photobleaching experiments. Sup35-GFP (2 μ M) was incubated with 20 mM PIPES, 50 mM NaCl, 3% PEG20K pH 6.0. A single pixel bleach spot was placed in the center of the drop, and the change in the local fluorescence was analyzed as a function of time. Size of droplets \sim 3 μ m. (H) Three-dimensional volume rendering of a *Sc. pombe* Sup35 droplet in 20 mM PIPES, 50 mM NaCl, 3% PEG20K pH 6.0 imaged with cryo-electron tomography. Scale bar, 50 nm.



was grown at 30°C in YE5 or EMM5 medium. A list of yeast strains is in table S2.

Plasmids and cloning

A list of plasmids used here can be found in table S2. Gateway cloning (Invitrogen) was carried out as described previously (41). *Sc. pombe* Sup35-mCherry was generated according to (42) using standard primers for amplification of the linear tagging cassette carrying the fluorescence protein tag. *Sc. pombe* was transformed with purified PCR product (43) and selected clones were verified using standard primers (42).

Energy depletion of cells

S. cerevisiae and *Sc. pombe* cells were energy depleted as described previously (16, 17). In short: Exponentially growing yeast were transferred to and incubated in liquid SC medium or EMM medium, respectively, without glucose containing 20 mM 2-deoxyglucose (2-DG, inhibition of glycolysis) and 10 μ M antimycin A (inhibition of mitochondrial ATP production). Treatment causes about 95% reduction in cellular ATP (44). Recovery of cells from energy depletion was by replacing energy depletion media with media containing 2% glucose. In a microfluidic setup (CellAsic), cells were grown for 2-3 hours with media prior to treatment. Medium was pumped with 2 PSI. Exchange of medium was carried out with 4 PSI for 2 min.

pH stress

Exponentially growing *S. cerevisiae* and *Sc. pombe* cells were transferred to 100 mM phosphate buffer of different pH containing 2 mM 2,4-dinitrophenol (DNP). Control samples were treated equally, but DNP was omitted. Cell recovery was by replacing buffer with medium containing 2% glucose. In a microfluidic setup (CellAsic), cells were grown for 2-3 hours prior to treatment. Medium was pumped with 2 PSI. Exchange of medium was at 4 PSI for 2 min.

Microscopy of yeast

Samples were prepared as described above. Imaging was with a DeltaVision (Applied Precision) microscope (Olympus IX70 stand, Osram Mercury short arc HBO light source, Olympus UPlanSApo 100x oil objective, CoolSnap HQ2 camera). Z stacks with 6 planes were collected. Imaging settings were: 5% excitation intensity, 0.15 s exposure time, 512x512 pixels, 2x2 binning.

FRAP measurements

In vivo and in vitro fluorescence recovery after photobleaching (FRAP) experiments were carried out with an Andor spinning disc microscope (Nikon TiE inverted stand, Nikon Apo 100x, NA 1.49 Oil objective, Andor iXon+ camera, EM gain 200, imaging laser intensity of 0.3% for reconstituted protein droplets and 5% for cells) equipped with a FRAPPA unit (Andor). A single pixel was bleached with a 405-nm laser pulse (1 repeat, 10% intensity, dwell time 10 ms). Recovery from photobleaching was recorded in a single focal plane. Image analysis was carried out in Fiji.

Ratiometric pH measurements

Cytosolic pH measurements were carried out as described in (16, 17). In short: pHluorin2 (45) was expressed in W303 ADE+ under control of a GPD promoter. pH calibration was obtained as described previously (16, 46). Imaging was carried

out using DAPI/FITC (Excitation: DAPI; Emission: FITC) and FITC/FITC (Excitation and emission: FITC) filter sets on a DeltaVision (Applied Precision) microscope (Olympus IX70 stand, Osram Mercury short arc HBO light source, 100x Olympus UPlanSApo objective, CoolSnap HQ2

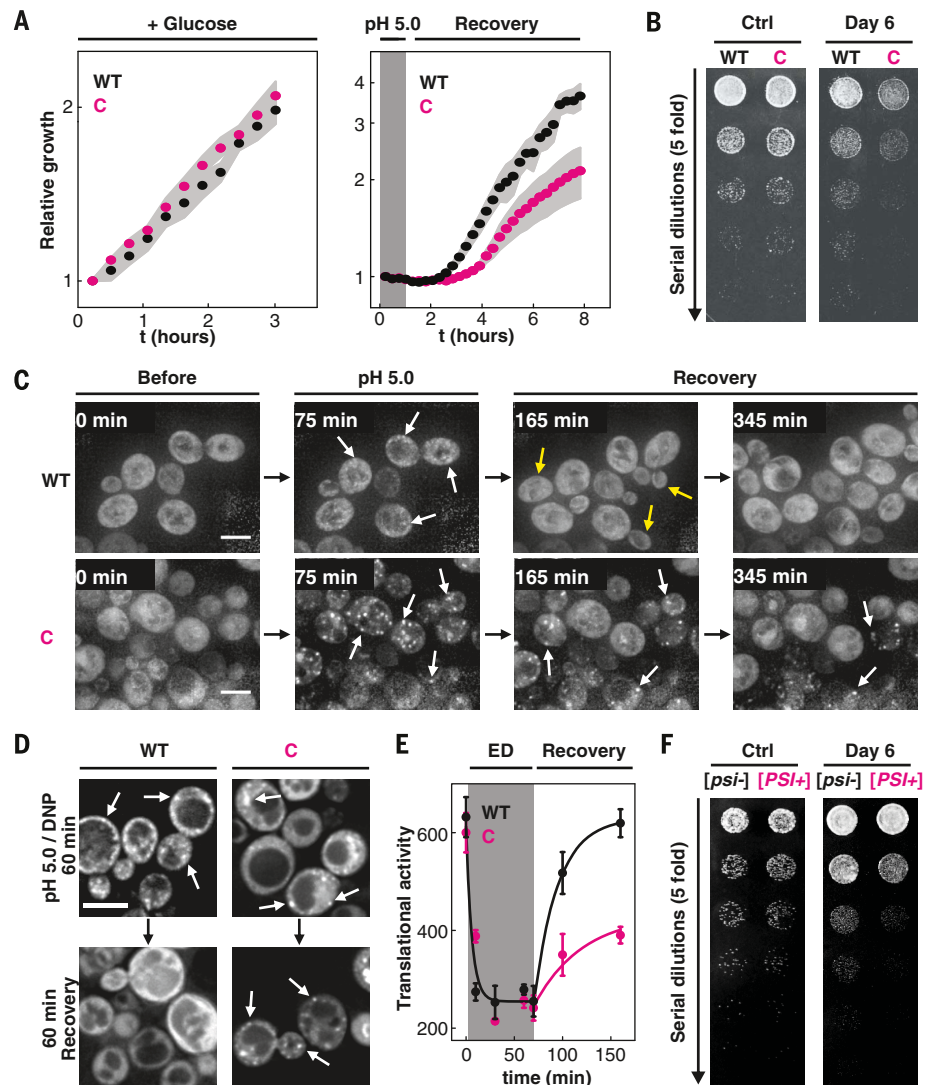


Fig. 4. The prion domain and a pH sensor work in synergy to protect the C domain from stress-induced damage. (A) Growth analysis of *S. cerevisiae* expressing WT Sup35 (black) or Sup35C (magenta) growing in synthetic complete medium in a microfluidic setup for 3 hours (left) and upon exposure to and recovery from pH 5.0/DNP for one hour (indicated in gray). SEM is shown in gray. *N* = 9 fields of view. (B) Spot-titer growth assay of *S. cerevisiae* expressing WT Sup35 (WT) and Sup35C (C) (Ctrl: exponentially growing cells were spotted) (left) and after recover from stationary phase. (C) Fluorescence images of *S. cerevisiae* expressing WT Sup35-GFP (top) and Sup35C-GFP (bottom) before (Before), during pH 5.0/DNP (pH 5.0), and during recovery (Recovery). WT Sup35-GFP particles dissolve rapidly during recovery, and cells grow and divide. Yellow arrows point toward newly formed yeast buds. Particles formed by Sup35C-GFP persist, and cells remain in an arrested state for a long time. Scale bars, 5 μ m. (D) Fluorescence images of *S. cerevisiae* expressing WT Sup35-GFP (left) and Sup35C-GFP (right) after exposure to pH 5.0/DNP for 60 min (top) and after 60 min of recovery (bottom). Arrows point toward Sup35 condensates. (E) Translational activity was determined for cells expressing WT Sup35 and Sup35C during exponential growth (first data point), during 60 min of energy depletion (ED; highlighted in gray) and during the recovery (Recovery). SD is shown; *N* = 500 to 700 cells per data point. (F) Spot-titer growth assay of the exponentially grown [*psi*⁻] and [*PSI*⁺] yeast (Ctrl) and cells that were grown to stationary phase cells for 6 days (Day 6).

camera). The mean DAPI/FITC to FITC/FITC ratio per cell was calculated from the intensity readouts and compared to the pH calibration.

Yeast growth assays

S. cerevisiae were grown overnight in YPD, diluted to OD₆₀₀ ~0.1 the next morning and regrown for two days. Stationary phase samples were taken every 24 hours over 20 days, spotted on YPD agar plates as five-fold serial dilutions. Plates were photographed 28 hours after spotting.

Semi-denaturing agarose-gel electrophoresis (SDD-AGE)

Yeast cells were grown to mid exponential phase in liquid rich medium at 30°C. Cells were washed with water and then subjected the following treatments: 2 hours 100 mM phosphate buffer pH 5.7, 2 mM DNP, 2 hours 100 mM phosphate buffer pH 7.5, 2 mM DNP, 2 hours energy depletion (20 mM 2-Deoxyglucose, 10 μM Antimycin A) and 10 min heat shock at 46°C. Cells were harvested by centrifugation and resuspended in 50 mM Tris, pH 7.5, 150 mM NaCl, 5 mM EDTA, 1% (v/v) Triton X-100, 30 mM NEM, 1 x Complete Protease Inhibitor (Roche). The cells were then lysed using glass beads (TissueLyser II from Qiagen, settings: 15 min, 25/sec) and were briefly spun at 2,000 rpm to sediment debris. 90 μl of supernatant were mixed with 4 × sample buffer (2 x TAE, 20% (v/v) glycerol, 4% (w/v) SDS, bromophenol blue). Samples were incubated at room temperature for 10 min and 50 μL were loaded onto a 1.5% agarose gel containing 1 x TAE and 0.1% SDS. The gel was run in 1 x TAE, 0.1% SDS at 100 V, followed by blotting onto a nitrocellulose membrane (GE Healthcare Life Sciences), as described in (47). Detection was with ECL plus solution (GE Healthcare Life Sciences) and a primary antibody against the C-terminal domain of Sup35 (Sup35C antibody kindly provided by R. Halfmann) and a secondary anti-mouse antibody.

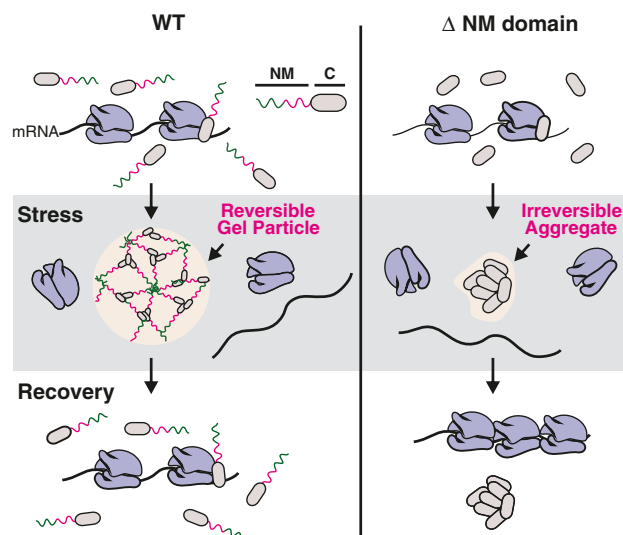
Polysome profiling

Polysome profiling was adapted as described in (48). In short: 250 mL yeast cultures were grown to OD₆₀₀ nm = 0.5. 100 mL were treated as untreated control sample, 150 mL were energy depleted as described above. After energy depletion, cycloheximide was added at a final concentration of 0.1 mg/ml to arrest polysomes and the samples were incubated on ice for 5 min. Cells were centrifuged 5 min at 3000 rpm and washed with 5 mL ice-cold polysome extraction buffer (PEB: 20 mM Tris-HCl pH7.4, 140 mM KCl, 5 mM MgCl₂, 0.1 mg/ml cycloheximide, 0.5 mM DTT, DECP treated H₂O). Cells were resuspended in 800 μL PEB, supplemented with 500 μL glass beads and lysed using a bead beater for 5 min at 30 Hz. The lysate was cleared by centrifugation for 5 min at 8000 × g, the absorbance at 260 nm was determined and an OD₂₆₀ nm of 20 of the supernatant were layered onto the sucrose gradient. The samples were subjected to ultracentrifugation for 2.5 hours at 35 krpm in an SW40 Ti rotor (Beckman). The

Fig. 5. The role of the Sup35 prion domain in stress adaptation.

Sup35 is soluble and catalyzes translation termination during growth. This function is independent of the N-proximal domain (NM) that comprises a prion domain (N, green) and a pH sensor domain (M, magenta). Stress, such as energy depletion, causes a decrease in intracellular pH (middle). The Sup35M domain senses changes in pH by protonation of negatively charged residues. This regulates interactions of the N-terminal prion domain

to form biomolecular condensates (left). The Sup35 condensates subsequently solidify into a protective gel-like meshwork sequestering the translation termination factor. In the absence of the disordered NM domain, the C domain undergoes irreversible aggregation (right). Upon cessation of stress, Sup35 gels readily dissolve, releasing the translation termination factor (bottom). The C domain persists in an aggregated state in the absence of the prion domain, thereby impairing protein translation.



gradients were subjected to UV 260 nm readings using a peristaltic pump.

Translation activity assay

Cells were grown to mid-log phase in SC medium. Samples were taken before, during after energy depletion at indicated time points. Newly synthesized proteins were labeled by resuspending the cells in SD medium depleted for methionine and supplemented with the methionine analog HPG (Invitrogen) for a 10-min pulse. Samples were fixed with 3.7% formaldehyde, washed twice with PBS and the cell wall was digested with Zymolyase (ZymoResearch). Cells were washed twice with PBS, 3% v/v BSA and permeabilized with 0.5% Triton X-100. Samples were mounted in 4-well dishes treated with polylysine. Click chemistry for HPG labeling was carried out according to the manufacture protocol (Click-iT, Invitrogen). Samples were imaged with a DeltaVision Elite as described above. Image analysis was carried out with Fiji.

Protein purification

Recombinant Sup35 and variants were expressed as N-terminal MBP-fusion proteins with a C-terminal His-Tag. Expression was by baculovirus expression in SF9 insect cells (3). Cells were lysed in buffer A (50 mM Tris-HCl, 1 M KCl, 2 mM EDTA, 1 mM DTT, pH 7.5) supplemented with cOmplete Protease Inhibitor Cocktail (Roche) using an Emulsiflex C5 (Avestin). Lysates were cleared by centrifugation (20,000 rpm, JA-25.50 rotor (Beckman Coulter), 60 min, 4°C). Supernatant was applied to MBP resin and washed with 20 column volumes buffer A. Elution was with 20 mM Maltose in buffer A. Samples were pooled and GST-tagged precision protease was added to cleave off the MBP- and His-tag and

dialyzed against buffer A overnight at 4°C. The sample was cleared by centrifugation and subjected to size exclusion chromatography using a Superdex-200 26/60 column (GE Healthcare Life Sciences) equilibrated with buffer A running on a BioCad 60 (Applied Biosystems) at RT. Pooled samples were concentrated and frozen in liquid nitrogen.

Reconstitution and microscopy of protein-rich droplets

Protein-rich droplets of Sup35 were formed by dilution of the protein from a stock solution into 20 mM PIPES, 2% Polyethylenglycol 20K. pH was adjusted with NaOH and the respective pH of the buffer is denoted in the figures and figure legends. Sup35 phase separation was tested at concentrations ranging from 0.1–20 μM. Phase diagrams were obtained at 2 μM Sup35. Samples were mixed in low-binding PCR vials and imaged on PEG-silane pacified microscopy slides and/or in 384 low-binding multi-well microscopy plates (Greiner Bio-One). Phase separation was scored yes or no, depending on the presence or absence of protein droplets. Samples for phase diagrams were imaged with a DeltaVision Elite (GE Healthcare Life Sciences), equipped with a multi-well plate holder using an Olympus UPlan SApochromat 100x, NA 1.4 Oil objective. Excitation of GFP labeled samples was at 488 nm and emission was at 520 nm. 20 μm z-stacks with 1 μm spacing were taken. For statistical representation and analysis 16 fields of views with a 50 μm spacing were recorded per sample. Enrichment measurements were carried out on an Andor spinning disc confocal microscope using a Nikon Apo 100x, NA 1.49 Oil objective on a Nikon TiE, inverted stand. Excitation was with a 488 nm DPSS laser.

Emission was recorded at 520 nm and detected with an Andor iXon EM+ DU-897 BV back illuminated EMCCD camera. 10 μm z-stacks with a spacing of 0.5 μm were taken. 9–16 field of views per sample were recorded. Image analysis was carried out with FIJI.

Cryo-electron microscopy and tomography

Copper Quantifoil grids (R2/1, Cu 200 mesh grid, Quantifoil Micro Tools) were glow discharged for 45 s and incubated with BSA-coated 15 nm gold nanoparticles. The solution was allowed to dry to adhere gold particles to the grid support and serve as fiducials for the alignment of tilt series. Phase separation was carried out immediately prior to the application of samples to the grids. 4 μl from each sample were deposited on grids and allowed to settle 30 s. Grids were plunge-frozen into liquid ethane/propane mixture at close to liquid nitrogen temperature using a Vitrobot Mark 4 (FEI). The blotting conditions were set to blot force 0.5–5 s blot time and 2 s drain time. Grids were stored in liquid nitrogen until usage. The blotting chamber conditions were set to 22°C, 90% humidity. Cryo-electron microscopy observations were performed on a Titan Krios operated at 300 kV (FEI), equipped with a field-emission gun, a Quantum post-column energy filter (Gatan) operated in the zero-loss mode, and a special heated phase plate holder (FEI). Data was recorded on a K2 Summit (Gatan) direct detector camera operated in dose fractionation mode. Electron micrographs were recorded under low-dose conditions (10–15 $e/\text{\AA}^2$) at EFTEM magnification of 42000 \times , corresponding to a pixel size 0.342 nm with target defocus of 4 μm . Individual frames acquired by K2 camera were aligned using an in-house implementation following procedures developed by Li *et al.* (49). Tilt-series were collected using SerialEM software (50). Tomography acquisition parameters were as follows: EFTEM magnification 42000 \times ; tilt range was $\pm 60^\circ$; tilt increment 2° ; total dose $\sim 60 e/\text{\AA}^2$; pixel size 0.342 nm. Data was acquired at target defocus of $-0.5 \mu\text{m}$ with a Volta phase plate. Alignment of tilt-series projection images was performed with gold nanoparticles as fiducials with IMOD software. Final alignment of the tilt-series images was performed using the linear interpolation option in IMOD and a low pass filter (cut off, 0.35; sigma, 0.05). No CTF correction was performed. Filtered volumes were generated in Matlab (Mathworks 2015) using TOM Toolbox and 3D rendered based on intensity threshold with the UCSF Chimera package (<http://www.cgl.ucsf.edu/chimera>).

Optical tweezer measurements

Controlled droplet fusion experiments were performed in a custom-built dual-trap optical tweezer microscope with two movable traps (51). At $t = 0$, phase separation of Sup35 droplets was induced. 10 μl of the reaction volume were applied and sealed in a static flow chamber (coverslip–double-sided tape–coverslip sandwich). Sample

preparation and mounting was carried out within 2–3 min. Protein droplets were trapped due to a mismatch in the index of refraction between droplets and buffer. The laser power of the 1064 nm trapping laser was kept at minimum ($<70 \text{ mW}$) to prevent heating artifacts. Keeping one optical trap stationary, the other optical trap was moved until droplets touched, after which droplet fusion was recorded with a temporal resolution of 1 ms (1 kHz). Apparent fusion times were derived from exponential fitting of the fusion traces and normalizing the apparent fusion time by the geometric radii of the droplets. Time of gelation at different conditions was measured by scoring successful and unsuccessful fusion events according to the following criteria: Fused droplet must relax to spherical shape within 30 s. Logistic regression was performed on the resulting curves.

Bioinformatics

Sequence analysis of Sup35 from *S. cerevisiae* and *Sc. pombe* was performed using localCIDER (52), IUPred (53), and the SuperFamily database (54). For each protein, six analysis tracks were generated. SupFam defines the functionally annotated domains, identifying the three well-characterized folded regions in the C-terminal domain. IUPred describes the degree of predicted disorder; the N and M domains are predicted to be disordered while the C domain is predicted to be folded. The remaining four tracks use a 20-residue sliding window to compute local sequence properties of relevance to disordered regions. FCR describes the fraction of charged residues and shows the N domain has relatively few charged residues while the M domain is substantially enriched. NCPR describes the net charge per residue. Despite substantial sequence divergence, the M domains have a characteristic charge distribution of a positively charged N-terminal region and a negatively charged C-terminal region. Hydro describes the local hydrophobicity using the Kyte-Doolittle hydrophobicity scale. Comparative charge distribution of various yeast species was also carried out using the emboss explorer charge module with a sliding window of 20-residues. Sequence identity analysis was carried out with ClustalOmega.

REFERENCES AND NOTES

- S. F. Banani, H. O. Lee, A. A. Hyman, M. K. Rosen, Biomolecular condensates: Organizers of cellular biochemistry. *Nat. Rev. Mol. Cell Biol.* **18**, 285–298 (2017). doi: [10.1038/nrm.2017.7](https://doi.org/10.1038/nrm.2017.7); pmid: [28225081](https://pubmed.ncbi.nlm.nih.gov/28225081/)
- C. P. Brangwynne *et al.*, Germline P granules are liquid droplets that localize by controlled dissolution/condensation. *Science* **324**, 1729–1732 (2009). doi: [10.1126/science.1172046](https://doi.org/10.1126/science.1172046); pmid: [19460965](https://pubmed.ncbi.nlm.nih.gov/19460965/)
- A. Patel *et al.*, A liquid-to-solid phase transition of the ALS protein FUS accelerated by disease mutation. *Cell* **162**, 1066–1077 (2015). doi: [10.1016/j.cell.2015.07.047](https://doi.org/10.1016/j.cell.2015.07.047); pmid: [26317470](https://pubmed.ncbi.nlm.nih.gov/26317470/)
- A. Mollie *et al.*, Phase separation by low complexity domains promotes stress granule assembly and drives pathological fibrillization. *Cell* **163**, 123–133 (2015). doi: [10.1016/j.cell.2015.09.015](https://doi.org/10.1016/j.cell.2015.09.015); pmid: [26406374](https://pubmed.ncbi.nlm.nih.gov/26406374/)
- J. A. Riback *et al.*, Stress-triggered phase separation is an adaptive, evolutionarily tuned response. *Cell* **168**, 1028–1040 (2017). doi: [10.1016/j.cell.2017.02.027](https://doi.org/10.1016/j.cell.2017.02.027); pmid: [28283059](https://pubmed.ncbi.nlm.nih.gov/28283059/)

- M. Kato *et al.*, Cell-free formation of RNA granules: Low complexity sequence domains form dynamic fibers within hydrogels. *Cell* **149**, 753–767 (2012). doi: [10.1016/j.cell.2012.04.017](https://doi.org/10.1016/j.cell.2012.04.017); pmid: [22579281](https://pubmed.ncbi.nlm.nih.gov/22579281/)
- D. M. Garcia, D. F. Jarosz, Rebels with a cause: Molecular features and physiological consequences of yeast prions. *FEMS Yeast Res.* **14**, 136–147 (2014). doi: [10.1111/1567-1364.12116](https://doi.org/10.1111/1567-1364.12116); pmid: [25667942](https://pubmed.ncbi.nlm.nih.gov/25667942/)
- R. Halfmann, S. Lindquist, Epigenetics in the extreme: Prions and the inheritance of environmentally acquired traits. *Science* **330**, 629–632 (2010). doi: [10.1126/science.1191081](https://doi.org/10.1126/science.1191081); pmid: [21030648](https://pubmed.ncbi.nlm.nih.gov/21030648/)
- R. Halfmann, S. Alberti, S. Lindquist, Prions, protein homeostasis, and phenotypic diversity. *Trends Cell Biol.* **20**, 125–133 (2010). doi: [10.1016/j.tcb.2009.12.003](https://doi.org/10.1016/j.tcb.2009.12.003); pmid: [20071174](https://pubmed.ncbi.nlm.nih.gov/20071174/)
- A. F. Harrison, J. Shorter, RNA-binding proteins with prion-like domains in health and disease. *Biochem. J.* **474**, 1417–1438 (2017). doi: [10.1042/BCJ20160499](https://doi.org/10.1042/BCJ20160499); pmid: [28389532](https://pubmed.ncbi.nlm.nih.gov/28389532/)
- R. B. Wickner, [URE3] as an altered URE2 protein: Evidence for a prion analog in *Saccharomyces cerevisiae*. *Science* **264**, 566–569 (1994). doi: [10.1126/science.7909170](https://doi.org/10.1126/science.7909170); pmid: [7909170](https://pubmed.ncbi.nlm.nih.gov/7909170/)
- P. Anderson, N. Kedersha, Stress granules. *Curr. Biol.* **19**, R397–R398 (2009). doi: [10.1016/j.cub.2009.03.013](https://doi.org/10.1016/j.cub.2009.03.013); pmid: [19467203](https://pubmed.ncbi.nlm.nih.gov/19467203/)
- J. R. Buchan, R. Parker, Eukaryotic stress granules: The ins and outs of translation. *Mol. Cell* **36**, 932–941 (2009). doi: [10.1016/j.molcel.2009.11.020](https://doi.org/10.1016/j.molcel.2009.11.020); pmid: [20064460](https://pubmed.ncbi.nlm.nih.gov/20064460/)
- J. Shorter, S. Lindquist, Hsp104 catalyzes formation and elimination of self-replicating Sup35 prion conformers. *Science* **304**, 1793–1797 (2004). doi: [10.1126/science.1098007](https://doi.org/10.1126/science.1098007); pmid: [15155912](https://pubmed.ncbi.nlm.nih.gov/15155912/)
- Y. Shin, C. P. Brangwynne, Liquid phase condensation in cell physiology and disease. *Science* **357**, eaaf4382 (2017). doi: [10.1126/science.aaf4382](https://doi.org/10.1126/science.aaf4382); pmid: [28935776](https://pubmed.ncbi.nlm.nih.gov/28935776/)
- M. C. Munder *et al.*, A pH-driven transition of the cytoplasm from a fluid- to a solid-like state promotes entry into dormancy. *eLife* **5**, 59–69 (2016). doi: [10.7554/eLife.09347](https://doi.org/10.7554/eLife.09347); pmid: [27003292](https://pubmed.ncbi.nlm.nih.gov/27003292/)
- I. Petrovska *et al.*, Filament formation by metabolic enzymes is a specific adaptation to an advanced state of cellular starvation. *eLife* **2014**, (2014). doi: [10.7554/eLife.02409](https://doi.org/10.7554/eLife.02409); pmid: [24771766](https://pubmed.ncbi.nlm.nih.gov/24771766/)
- B. R. Parry *et al.*, The bacterial cytoplasm has glass-like properties and is fluidized by metabolic activity. *Cell* **156**, 183–194 (2014). doi: [10.1016/j.cell.2013.11.028](https://doi.org/10.1016/j.cell.2013.11.028); pmid: [24361104](https://pubmed.ncbi.nlm.nih.gov/24361104/)
- S. Saha *et al.*, Polar positioning of phase-separated liquid compartments in cells regulated by an mRNA competition mechanism. *Cell* **166**, 1572–1584 (2016). doi: [10.1016/j.cell.2016.08.006](https://doi.org/10.1016/j.cell.2016.08.006); pmid: [27594427](https://pubmed.ncbi.nlm.nih.gov/27594427/)
- T. R. Serio *et al.*, Nucleated conformational conversion and the replication of conformational information by a prion determinant. *Science* **289**, 1317–1321 (2000). doi: [10.1126/science.289.5483.1317](https://doi.org/10.1126/science.289.5483.1317); pmid: [10958771](https://pubmed.ncbi.nlm.nih.gov/10958771/)
- S. Alberti, R. Halfmann, O. King, A. Kapila, S. Lindquist, A systematic survey identifies prions and illuminates sequence features of prionogenic proteins. *Cell* **137**, 146–158 (2009). doi: [10.1016/j.cell.2009.02.044](https://doi.org/10.1016/j.cell.2009.02.044); pmid: [19345193](https://pubmed.ncbi.nlm.nih.gov/19345193/)
- I. Stansfield *et al.*, The products of the SUP45 (eRF1) and SUP35 genes interact to mediate translation termination in *Saccharomyces cerevisiae*. *EMBO J.* **14**, 4365–4373 (1995). pmid: [7556078](https://pubmed.ncbi.nlm.nih.gov/7556078/)
- M. D. Ter-Avanesyan *et al.*, Deletion analysis of the SUP35 gene of the yeast *Saccharomyces cerevisiae* reveals two non-overlapping functional regions in the encoded protein. *Mol. Microbiol.* **7**, 683–692 (1993). doi: [10.1111/j.1365-2958.1993.tb01159.x](https://doi.org/10.1111/j.1365-2958.1993.tb01159.x); pmid: [8469113](https://pubmed.ncbi.nlm.nih.gov/8469113/)
- Y. O. Chernoff *et al.*, Evolutionary conservation of prion-forming abilities of the yeast Sup35 protein. *Mol. Microbiol.* **35**, 865–876 (2000). doi: [10.1046/j.1365-2958.2000.01761.x](https://doi.org/10.1046/j.1365-2958.2000.01761.x); pmid: [10692163](https://pubmed.ncbi.nlm.nih.gov/10692163/)
- H. K. Edskes *et al.*, Sporadic distribution of prion-forming ability of Sup35p from yeasts and fungi. *Genetics* **198**, 605–616 (2014). doi: [10.1534/genetics.114.166538](https://doi.org/10.1534/genetics.114.166538); pmid: [25081567](https://pubmed.ncbi.nlm.nih.gov/25081567/)
- T. K. Harris, G. J. Turner, Structural basis of perturbed pKa values of catalytic groups in enzyme active sites. *J. Biol. Chem.* **285**, 85–98 (2010). doi: [10.1074/jbc.M109.021146](https://doi.org/10.1074/jbc.M109.021146); pmid: [20492000](https://pubmed.ncbi.nlm.nih.gov/20492000/)
- F. Ruggeri *et al.*, Single-molecule electrometry. *Nat. Nanotechnol.* **12**, 488–495 (2017). doi: [10.1038/nnano.2017.26](https://doi.org/10.1038/nnano.2017.26); pmid: [28288117](https://pubmed.ncbi.nlm.nih.gov/28288117/)

28. J. R. Glover *et al.*, Self-seeded fibers formed by Sup35, the protein determinant of [PSI⁺], a heritable prion-like factor of *S. cerevisiae*. *Cell* **89**, 811–819 (1997). doi: [10.1016/S0092-8674\(00\)80264-0](https://doi.org/10.1016/S0092-8674(00)80264-0); pmid: [9182769](https://pubmed.ncbi.nlm.nih.gov/9182769/)
29. M. Rubinstein, A. N. Semenov, Thermoreversible gelation in solutions of associating polymers. 2. Linear dynamics. *Macromolecules* **31**, 1386–1397 (1998). doi: [10.1021/ma970617+](https://doi.org/10.1021/ma970617+)
30. T. S. Harmon, A. S. Holehouse, M. K. Rosen, R. V. Pappu, Intrinsically disordered linkers determine the interplay between phase separation and gelation in multivalent proteins. *eLife* **6**, e30294 (2017). doi: [10.7554/eLife.30294](https://doi.org/10.7554/eLife.30294); pmid: [29091028](https://pubmed.ncbi.nlm.nih.gov/29091028/)
31. M.-T. Wei *et al.*, Phase behaviour of disordered proteins underlying low density and high permeability of liquid organelles. *Nat. Chem.* **9**, 1118–1125 (2017). doi: [10.1038/nchem.2803](https://doi.org/10.1038/nchem.2803); pmid: [29064502](https://pubmed.ncbi.nlm.nih.gov/29064502/)
32. L. Z. Osherovich, J. S. Weissman, Multiple Gln/Asn-rich prion domains confer susceptibility to induction of the yeast [PSI⁺] prion. *Cell* **106**, 183–194 (2001). doi: [10.1016/S0092-8674\(01\)00440-8](https://doi.org/10.1016/S0092-8674(01)00440-8); pmid: [11511346](https://pubmed.ncbi.nlm.nih.gov/11511346/)
33. S. V. Paushkin, V. V. Kushnir, V. N. Smirnov, M. D. Ter-Avanesyan, Propagation of the yeast prion-like [psi⁺] determinant is mediated by oligomerization of the SUP35-encoded polypeptide chain release factor. *EMBO J.* **15**, 3127–3134 (1996). pmid: [8670813](https://pubmed.ncbi.nlm.nih.gov/8670813/)
34. R. P. McGlinchey, D. Kryndushkin, R. B. Wickner, Suicidal [PSI⁺] is a lethal yeast prion. *Proc. Natl. Acad. Sci. U.S.A.* **108**, 5337–5341 (2011). doi: [10.1073/pnas.1102762108](https://doi.org/10.1073/pnas.1102762108); pmid: [21402947](https://pubmed.ncbi.nlm.nih.gov/21402947/)
35. R. B. Wickner, D. C. Masison, H. K. Edskes, [PSI⁺] and [URE3] as yeast prions. *Yeast* **11**, 1671–1685 (1995). doi: [10.1002/yea.320111609](https://doi.org/10.1002/yea.320111609); pmid: [8720070](https://pubmed.ncbi.nlm.nih.gov/8720070/)
36. T. Nakayashiki, C. P. Kurtzman, H. K. Edskes, R. B. Wickner, Yeast prions [URE3] and [PSI⁺] are diseases. *Proc. Natl. Acad. Sci. U.S.A.* **102**, 10575–10580 (2005). doi: [10.1073/pnas.0504882102](https://doi.org/10.1073/pnas.0504882102); pmid: [16024723](https://pubmed.ncbi.nlm.nih.gov/16024723/)
37. R. B. Wickner, H. K. Edskes, D. Bateman, A. C. Kelly, A. Gorkovskiy, The yeast prions [PSI⁺] and [URE3] are molecular degenerative diseases. *Prion* **5**, 258–262 (2011). doi: [10.4161/pri.17748](https://doi.org/10.4161/pri.17748); pmid: [22052353](https://pubmed.ncbi.nlm.nih.gov/22052353/)
38. Y. O. Chernoff, Stress and prions: Lessons from the yeast model. *FEBS Lett.* **581**, 3695–3701 (2007). doi: [10.1016/j.febslet.2007.04.075](https://doi.org/10.1016/j.febslet.2007.04.075); pmid: [17509571](https://pubmed.ncbi.nlm.nih.gov/17509571/)
39. L. Malinowska, S. Alberti, Protein misfolding in *Dictyostelium*: Using a freak of nature to gain insight into a universal problem. *Prion* **9**, 339–346 (2015). doi: [10.1080/19336896.2015.1099799](https://doi.org/10.1080/19336896.2015.1099799); pmid: [26529309](https://pubmed.ncbi.nlm.nih.gov/26529309/)
40. L. Malinowska, S. Palm, K. Gibson, J.-M. Verbavatz, S. Alberti, *Dictyostelium discoideum* has a highly Q/N-rich proteome and shows an unusual resilience to protein aggregation. *Proc. Natl. Acad. Sci. U.S.A.* **112**, E2620–E2629 (2015). doi: [10.1073/pnas.1504459112](https://doi.org/10.1073/pnas.1504459112); pmid: [25941378](https://pubmed.ncbi.nlm.nih.gov/25941378/)
41. S. Alberti, A. D. Gitler, S. Lindquist, A suite of Gateway cloning vectors for high-throughput genetic analysis in *Saccharomyces cerevisiae*. *Yeast* **24**, 913–919 (2007). doi: [10.1002/yea.1502](https://doi.org/10.1002/yea.1502); pmid: [17583893](https://pubmed.ncbi.nlm.nih.gov/17583893/)
42. J. Bähler *et al.*, Heterologous modules for efficient and versatile PCR-based gene targeting in *Schizosaccharomyces pombe*. *Yeast* **14**, 943–951 (1998). doi: [10.1002/\(SICI\)1097-0061\(199807\)14:10<943::AID-YEA292>3.0.CO;2-Y](https://doi.org/10.1002/(SICI)1097-0061(199807)14:10<943::AID-YEA292>3.0.CO;2-Y); pmid: [9717240](https://pubmed.ncbi.nlm.nih.gov/9717240/)
43. S. L. Forsburg, N. Rhind, Basic methods for fission yeast. *Yeast* **23**, 173–183 (2006). doi: [10.1002/yea.1347](https://doi.org/10.1002/yea.1347); pmid: [16498704](https://pubmed.ncbi.nlm.nih.gov/16498704/)
44. R. Serrano, Energy requirements for maltose transport in yeast. *Eur. J. Biochem.* **80**, 97–102 (1977). doi: [10.1111/j.1432-1033.1977.tb11861.x](https://doi.org/10.1111/j.1432-1033.1977.tb11861.x); pmid: [21792](https://pubmed.ncbi.nlm.nih.gov/21792/)
45. M. J. Mahon, pHluorin2: An enhanced, ratiometric, pH-sensitive green fluorescent protein. *Adv. Biosci. Biotechnol.* **2**, 132–137 (2011). doi: [10.4236/abb.2011.23021](https://doi.org/10.4236/abb.2011.23021); pmid: [21841969](https://pubmed.ncbi.nlm.nih.gov/21841969/)
46. C. L. Brett, D. N. Tukaye, S. Mukherjee, R. Rao, The yeast endosomal Na⁺/K⁺/H⁺ exchanger Nhx1 regulates cellular pH to control vesicle trafficking. *Mol. Biol. Cell* **16**, 1396–1405 (2005). doi: [10.1091/mbc.E04-11-0999](https://doi.org/10.1091/mbc.E04-11-0999); pmid: [15635088](https://pubmed.ncbi.nlm.nih.gov/15635088/)
47. R. Halfmann, S. Lindquist, Screening for amyloid aggregation by semi-denaturing detergent-agarose gel electrophoresis. *J. Vis. Exp.* **17**, e838 (2008). pmid: [19066511](https://pubmed.ncbi.nlm.nih.gov/19066511/)
48. T. Mašek, L. Valášek, M. Pospíšek, in *RNA: Methods in Molecular Biology (Methods and Protocols)*, vol. 703, H. Nielsen, Ed. (Humana Press, 2011), pp. 293–309.
49. X. Li *et al.*, Electron counting and beam-induced motion correction enable near-atomic-resolution single-particle cryo-EM. *Nat. Methods* **10**, 584–590 (2013). doi: [10.1038/nmeth.2472](https://doi.org/10.1038/nmeth.2472); pmid: [23644547](https://pubmed.ncbi.nlm.nih.gov/23644547/)
50. D. N. Mastrorade, Automated electron microscope tomography using robust prediction of specimen movements. *J. Struct. Biol.* **152**, 36–51 (2005). doi: [10.1016/j.jsb.2005.07.007](https://doi.org/10.1016/j.jsb.2005.07.007); pmid: [16182563](https://pubmed.ncbi.nlm.nih.gov/16182563/)
51. M. Jahnel, M. Behrndt, A. Jannasch, E. Schäffer, S. W. Grill, Measuring the complete force field of an optical trap. *Opt. Lett.* **36**, 1260–1262 (2011). doi: [10.1364/OL.36.001260](https://doi.org/10.1364/OL.36.001260); pmid: [21479051](https://pubmed.ncbi.nlm.nih.gov/21479051/)
52. A. S. Holehouse, R. K. Das, J. N. Ahad, M. O. G. Richardson, R. V. Pappu, CIDER: Resources to analyze sequence-ensemble relationships of intrinsically disordered proteins. *Biophys. J.* **112**, 16–21 (2017). doi: [10.1016/j.bpj.2016.11.3200](https://doi.org/10.1016/j.bpj.2016.11.3200); pmid: [28076807](https://pubmed.ncbi.nlm.nih.gov/28076807/)
53. Z. Dosztányi, V. Csizsmok, P. Tompa, I. Simon, IUPred: Web server for the prediction of intrinsically unstructured regions of proteins based on estimated energy content. *Bioinformatics* **21**, 3433–3434 (2005). doi: [10.1093/bioinformatics/bti541](https://doi.org/10.1093/bioinformatics/bti541); pmid: [15955779](https://pubmed.ncbi.nlm.nih.gov/15955779/)
54. J. Gough, K. Karplus, R. Hughey, C. Chothia, Assignment of homology to genome sequences using a library of hidden Markov models that represent all proteins of known structure. *J. Mol. Biol.* **313**, 903–919 (2001). doi: [10.1006/jmbi.2001.5080](https://doi.org/10.1006/jmbi.2001.5080); pmid: [11697912](https://pubmed.ncbi.nlm.nih.gov/11697912/)

ACKNOWLEDGMENTS

We thank the following Services and Facilities of the Max Planck Institute of Molecular Cell Biology and Genetics (MPI-CBG) for their support: We thank B. Borgonovo and R. Lemaitre (Protein Expression Purification and Characterization) for help with protein expression and purification; B. Nitzsche and B. Schroth-Diez (Light Microscopy Facility) for help with light microscopy; F. Friedrich for support with visualization (Media Technologies and Outreach); and C. Iserman for a yeast strain BY4742 coexpressing Sup35-GFP and Pab1-mCherry. We thank members of the MPI-CBG and C. Weber from the Max Planck Institute for the Physics of Complex systems for discussion and comments on the manuscript. R. Halfmann is acknowledged for providing the antibody against Sup35C domain. We gratefully acknowledge funding from the German Federal Ministry of Research and Education (BMBF O31A359A to T.M.F. and A.A.H.). This work is supported by the MaxSynBio consortium, jointly funded by the Federal Ministry of Education and Research of Germany and the Max Planck Society. We further acknowledge the U.S. National Institutes of Health for grant 5R01NS056114 to R.V.P., The Human Frontiers Program for grant RGP0034/2017 to S.A. and R.V.P., the Volkswagen “Life?” initiative for a grant to S.A., and the German Research Foundation (DFG) for a grant to S.A. All the data relevant to this study are included in the main paper or the supplementary materials.

SUPPLEMENTARY MATERIALS

www.sciencemag.org/content/359/6371/eaao5654/suppl/DC1

Figs. S1 to S5

Tables S1 and S2

Movies S1 to S8

3 August 2017; accepted 27 November 2017

10.1126/science.aao5654